SANDIA REPORT

SAND2015-7870
Unlimited Release
Printed September 2015

Creating physically-based three-dimensional microstructures: Bridging phase-field and crystal plasticity models

Hojun Lim, Steven Owen, Fadi Abdeljawad, Byron Hanks and Corbett Battaile

Prepared by
Sandia National Laboratories
Albuquerque, New Mexico 87185 and Livermore, California 94550

Sandia National Laboratories is a multi-program laboratory managed and operated by Sandia Corporation, a wholly owned subsidiary of Lockheed Martin Corporation, for the U.S. Department of Energy's National Nuclear Security Administration under contract DE-AC04-94AL85000.

Sandia National Laboratories

Issued by Sandia National Laboratories, operated for the United States Department of Energy by Sandia Corporation.

Available to DOE and DOE contractors from
U.S. Department of Energy
Office of Scientific and Technical Information
P.O. Box 62
Oak Ridge, TN 37831

Telephone: (865) 576-8401
Facsimile: (865) 576-5728
E-Mail: reports@adonis.osti.gov
Online ordering: http://www.osti.gov/bridge

Available to the public from
U.S. Department of Commerce
National Technical Information Service
5285 Port Royal Rd
Springfield, VA 22161

Telephone: (800) 553-6847
Facsimile: (703) 605-6900
E-Mail: orders@ntis.fedworld.gov
Online ordering: http://www.ntis.gov/help/ordermethods.asp?loc=7-4-0#online

SAND2015-7870
Unlimited Release
Printed September 2015

Creating physically-based three-dimensional microstructures: Bridging phase-field and crystal plasticity models

Hojun Lim, Fadi Abdeljawad and Corbett Battaile
Computational Materials and Data Science,
Sandia National Laboratories, Albuquerque, NM 87185

Steven Owen and Byron Hanks
Metallurgy and Materials Joining,
Sandia National Laboratories, Albuquerque, NM 87185

Abstract

In order to better incorporate microstructures in continuum scale models, we use a novel finite element (FE) meshing technique to generate three-dimensional polycrystalline aggregates from a phase field grain growth model of grain microstructures. The proposed meshing technique creates hexahedral FE meshes that capture smooth interfaces between adjacent grains. Three dimensional realizations of grain microstructures from the phase field model are used in crystal plasticity-finite element (CP-FE) simulations of polycrystalline α-iron. We show that the interface conformal meshes significantly reduce artificial stress localizations in voxelated meshes that exhibit the so-called "wedding cake" interfaces. This framework provides a direct link between two mesoscale models - phase field and crystal plasticity - and for the first time allows mechanics simulations of polycrystalline materials using three-dimensional hexahedral finite element meshes with realistic topological features.

Acknowledgment

This work is supported by LDRD (15-1674 and 15-0764), Predicting Performance Margins (PPM) and Advanced Simulation and Computing - Physics and Engineering Models (ASC-P&EM) programs at Sandia National Laboratories. Sandia National Laboratories is a multi-program laboratory managed and operated by Sandia Corporation, a wholly owned subsidiary of Lockheed Martin Corporation, for the U.S. Department of Energy's National Nuclear Security Administration under contract DE-AC04-94AL85000.

Contents

Figures

Tables

1 Introduction

Nearly all metallic materials used in every engineering application are composed of many grains. Most engineering-scale continuum models, however, ignore heterogeneous material properties arising from individual grains and use homogeneous, averaged properties from measurements on polycrystals. Meso-scale models, e.g. crystal plasticity (CP), use constitutive descriptions applied to individual grains and thus microstructural effects, e.g. grain morphology (grain size and shape) and texture (grain orientation), are directly considered. CP models are now widely implemented into finite element method (CP-FEM) and are used to simulate deformations of polycrystals to predict texture and mechanical responses [25, 15, 4, 11, 27, 10, 32]. In these finite element (FE)-based models, it is critical to accurately reproduce realistic three dimensional microstructures. However, accurate modeling of polycrystalline material is hindered by two significant shortcomings in the current capabilities to reproduce realistic three dimensional grain-scale microstructures.

Most FE-based polycrystalline models use idealized grain shapes or Voronoi tessellations (Figure 1 (b)) to create three dimensional microstructures as [7, 5, 31, 22]. In principle, there are no topological constraints on the resulting Voronoi polyhedral cells or grains. As a result, these methods fail to satisfy several geometrical characteristics that are present in real microstructures. For example, in isotropic systems the equilibrium angles at triple junctions, where three grains meet, are all 120° (the Herring condition). In addition, distributions of the number of faces and edges obey specific criteria in nature (Euler's rules). More realistic three dimensional microstructure can be reproduced with considerations of materials and physics, i.e. surface energies and/or energy minimizing shapes, using the grain growth phase field model. A three dimensional phase field grain growth model provides more physically-based microstructures that resembles real microstructure as shown in Figure 1 (a) and (c).

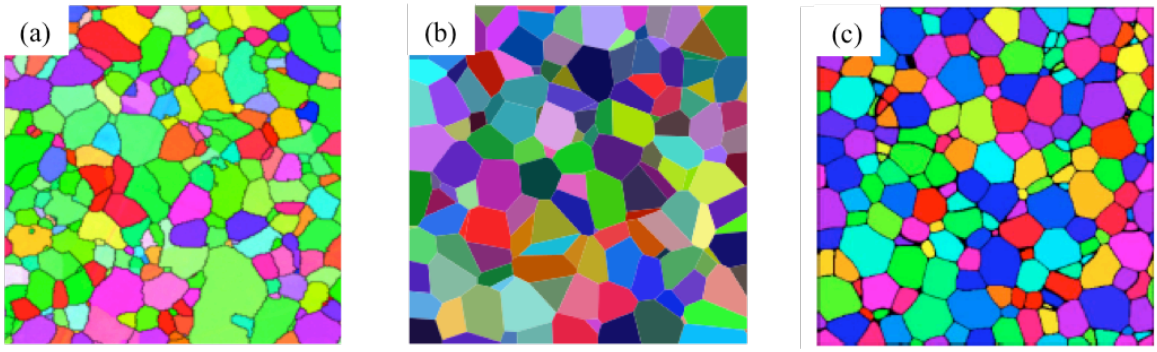

Figure 1. Polycrystalline microstructures from (a) electron back scatter diffraction (EBSD), (b) Voronoi tesselation and (c) phase field grain growth model.

A 3D microstructure constructed from experiments (serial sectioning EBSD) or computational tools, i.e. phase field or Monte Carlo grain growth models, usually conforms to a uniform grid.

Thus, CP-FEM polycrystalline models generated from these data generally have cubic hexahedral elements. However, representing microstructural features using cubic finite elements leads to voxelated surfaces, or the so-called wedding cake interfaces [7]. This problem cannot be easily corrected by refining the mesh. Instead, conforming smooth boundaries at microstructural features, i.e. grain boundaries, are required to eliminate the artifacts that arise from voxelated geometries. This becomes more important if we consider highly localized events, e.g. crack initiation, damage and fracture. However, Sandias meshing tools (Cubit) as well as existing commercial software (DREAM.3-D) do not yet have a capability to create splined three dimensional meshes using data from either simulations or experiments. Previously, polycrystalline mesh using tetrahedral finite elements are proposed [26] but hexahedral finite elements are usually favored in many FE applications.

In this work, we use a novel meshing technique in Cubit Meshing and Geometry Toolkit to create three dimensional finite element meshes of polycrystalline materials from grid based phase-field grain growth model. Enhanced Sculpt feature in Cubit creates hexahedral finite element meshes that conform to internal interfaces or grain boundaries. Generated mesh is then use to conduct mechanical simulations of polycrystalline α-iron via CP-FEM model. Effects of conformal mesh on the local and global response of polycrystalline behavior is discussed.

2 Procedure

2.1 Conformal meshing technique

To generate a conformal mesh from a uniform grid of phase field data, the Sculpt meshing tool [24] is used. Sculpt is a companion application to the Cubit Meshing and Geometry Toolkit developed at Sandia National Laboratories. It is a parallel all-hex tool that utilizes an overlay grid procedure where smooth conforming grain interfaces are extracted from phase field volume fractions. The procedure is briefly outlined in Figures 2 (a) to 2 (d). Figure 2 (a) shows an example of Cartesian grid of volume fractions where v_i is the volume fraction of the i^{th} grain contained within each grid cell. Thus, $\sum v_i = 1.0$ is satisfied. Grain interfaces are approximated using a procedure described in [24] and grid nodes are moved to the interfaces as shown in 2 (b). Figure 2 (c) then shows a layer of hexahedra inserted on both sides of the grain interfaces by projecting orthogonally from the local interface tangent plane. To improve mesh quality, a smoothing step is performed to improve both smoothness of the interface plains and the quality of the hexahedra as shown in figure 2 (d). Figure 3 shows schematics of the pillowing procedure that improves mesh quality at interfaces.

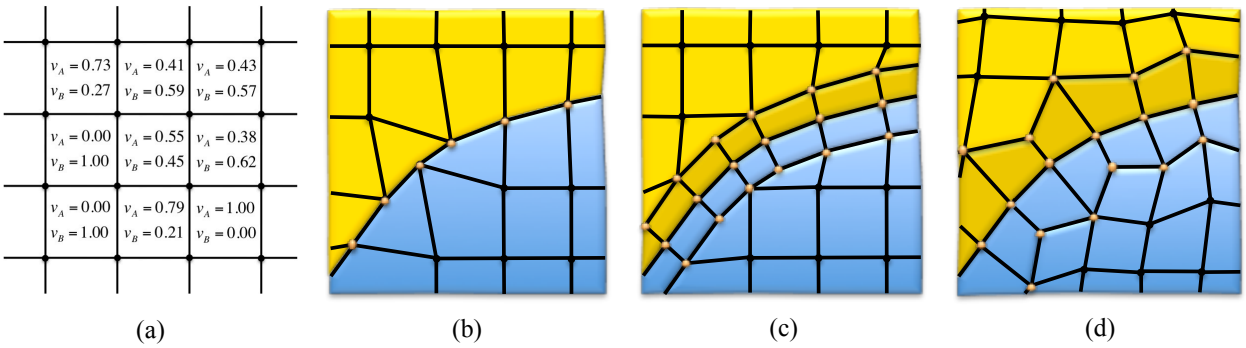

Figure 2. Schematics of the conformal meshing procedure: (a) Volume fractions representing percent of grains filling each cell in Cartesian grid, (b) grain interfaces are resolved and nodes projected to surfaces, (c) layer of hex element inserted on both sides of interface surfaces and (d) smoothing performed on curves, surfaces and volume nodes.

The above procedure allows for cases where multiple grains meet at common interfaces. To accommodate this, an underlying boundary representation (B-Rep) consisting of vertices, curves, surfaces and volumes is constructed which serve as the basis for smoothing operations. Nodes on curves are smoothed and projected to a Hermite approximation of the surrounding curve nodes. Surfaces are then smoothed using a Laplacian smoothing procedure. Volume nodes are then smoothed using a combined Laplacian and Optimization-based procedure described in [23]. Several iterations of curve, surface and volume smoothing are performed until a minimum mesh quality metric is achieved.

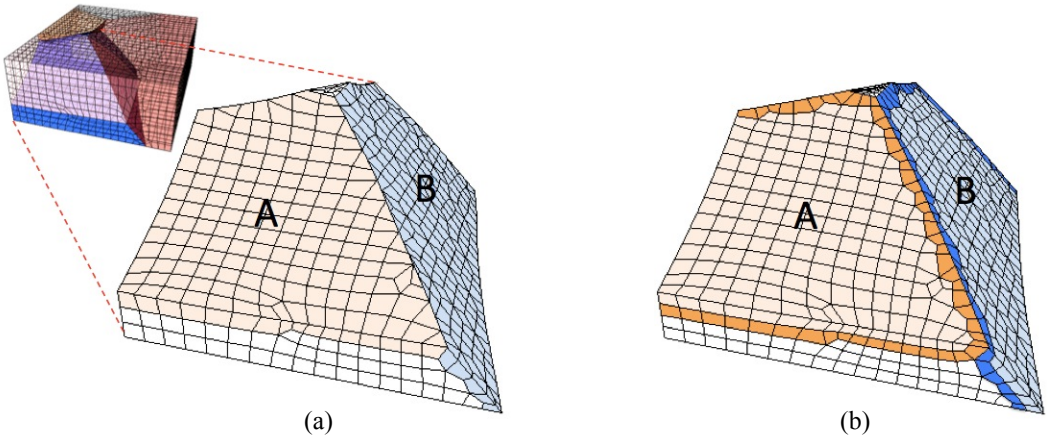

Figure 3. Schematics of the pillowing procedure: (a) Initial mesh at curve interfaces may be poor. Note triangle shaped quad faces between surfaces A and B. (b) Pillow layers of hexes are inserted srrounding all hexes sharing a common surface. Darker hexes indicate pillow layers. Note improved quad faces at curve between surfaces A and B compared to (a).

As mesh quality is a critical factor in this procedure, we note instances where the grain interfaces may intersect the domain boundary at very small angles consequently resulting in hexes that also have very small dihedral angles as shown in Figure 4 (a). To address this issue, Figure 4 (b) illustrates where additional layers of Cartesian cells can be added at the boundary of the domain. To facilitate this, volume fractions from the original boundary are copied to the new layers. This results in interfaces that intersect with the boundary at angles closer to ninety degrees, resulting in improved quality hexes.

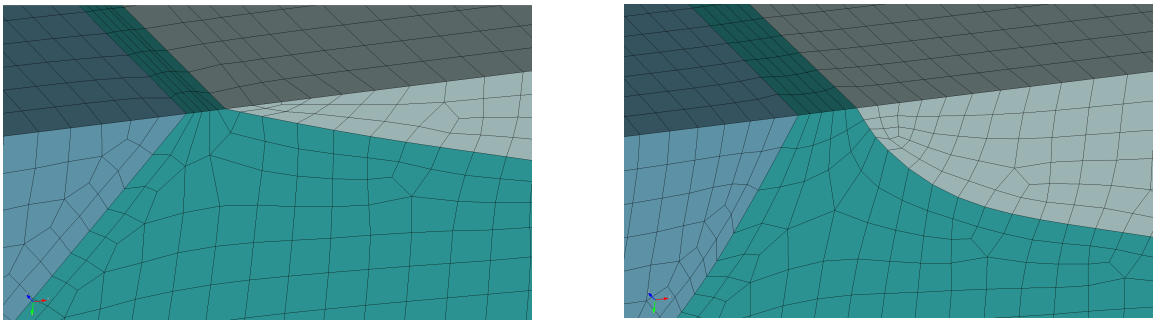

(a) (b)

Figure 4. Mesh quality improvements: (a) Poor quality hexes may result where grain interfaces intersect domain boundaries at small angles. (b) Additional layers of cells added to the domain boundaries result in improved quality for case illustrated in (a).

2.2 Phase field grain growth model

We employ a recently developed phase field model of grain microstructures to generate polycrystalline systems with various features of the grains. The model is briefly outlined here and the reader is referred to [2, 1] for more details on the model. The starting point of the phase field model for grain microstructures is the introduction of structural order parameters (OPs) $\{\phi_i(\mathbf{r},t), i = 1,\cdots,n_\phi\}$ that describe grains with various crystallographic orientations. Here, $\mathbf{r}, t, n_\phi$ denote the position vector, time and number of OPs needed to resolve the microstructure, respectively. Next, a coarse-grained free energy functional of a polycrystalline system, $\mathscr{F}_{tot}$, is proposed

$$\mathscr{F}_{tot} = \int d\mathbf{r} \left[W_\phi f_{grain}(\phi_i) + \sum_i^{n_\phi} \frac{\varepsilon_i^2}{2} |\nabla \phi_i|^2 \right], \tag{1}$$

where $f_{grain}(\phi_i) = f_{grain}(\{\phi_i(\mathbf{r},t), i = 1,\cdots,n_\phi\})$ is the homogeneous free energy density and W_ϕ is a parameter that sets the energy scale. The second term on the right hand side of Eq. (1) describes grain boundary (GB) energy, where under the isotropy assumption $\varepsilon_i = \varepsilon$. The OPs are conveniently chosen such that the equilibrium values within a grain $\{\phi_i(\mathbf{r},t) = 1, \phi_{j\neq i}(\mathbf{r},t) = 0, i, j = 1,\cdots,n_\phi\}$. Herein, we adopt the following form for the free energy density of a grain microstructure

$$f_{grain} = \frac{4}{3} \left[1 - 4 \sum_{i=1}^{n_\phi} \phi_i^3 + 3 \left(\sum_{i=1}^{n_\phi} \phi_i^2 \right)^2 \right], \tag{2}$$

where again the minima of f_{grain} are located at $\{\phi_i\} = \{1,0,\cdots,0\} = \cdots = \{0,0,\cdots,1\}$.

Within the Ginzburg-Landau formalism and with the aid of variational principles, the spatio-temporal evolution of the OPs $\{\phi_i(\mathbf{r},t), i = 1,\cdots,n_\phi\}$ follows from the Allen-Cahn equation [3]:

$$\frac{\partial \phi_i}{\partial t} = -L_i \left(\frac{\delta \mathscr{F}_{tot}}{\delta \phi_i} \right), \; i = 1,\cdots,n_\phi, \tag{3}$$

where under the isotropy assumption the model parameters $L_i = L$, one for each ϕ_i, control GB mobility. Within this treatment, the GB energy, γ_{gb}, width, δ_{gb}, and mobility, M_{gb}, are uniquely determined via [1].

$$\gamma_{gb} = \frac{2\sqrt{2}}{3} \varepsilon \sqrt{W_\phi}, \tag{4}$$

$$\delta_{gb} \simeq \frac{1.1}{\sqrt{2}} \frac{\varepsilon}{\sqrt{W_\phi}}, \tag{5}$$

$$M_{gb}\gamma_{gb} = L\varepsilon^2. \tag{6}$$

2.3 Crystal plasticity finite element model

In this work, BCC crystal plasticity finite element model developed at Sandia National Laboratories [21, 20] was used to simulate plastic deformations of polycrystalline α-iron. Crystal plasticity models use constitutive descriptions and crystal orientations applied to individual grains and impose plastic slip along the specified slip systems. The model is based on a well-established continuum formulation following a multiplicative decomposition of the deformation gradient [17, 28, 13, 25, 12, 19, 18]. Assuming plastic deformation is caused by dislocation slip, the plastic part of the velocity gradient, $\mathbf{L}_\mathrm{p}$, can be written as [25]:

$$\mathbf{L}_\mathrm{p} = \sum_\alpha \dot{\gamma}^\alpha \mathbf{s}_0^\alpha \otimes \mathbf{n}_0^\alpha, \tag{7}$$

where $\mathbf{s}_0^\alpha$ and $\mathbf{n}_0^\alpha$ are the initial slip direction and the slip plane normal direction on α-th slip system, respectively. Here, 24 $\{110\}\langle 111\rangle$ slip systems are used and for simplicity, non-Schmid effects are neglected. The slip rate on α-th slip system, $\dot{\gamma}^\alpha$, is represented as a power-law function of resolved shear stress, τ^α and slip resistance, g^α [14]:

$$\dot{\gamma}^\alpha = \dot{\gamma}_0^\alpha \left(\frac{\tau^\alpha}{g^\alpha} \right)^{1/m}. \tag{8}$$

where, $\dot{\gamma}_0^\alpha$ is the reference shear rate and m is the rate sensitivity factor. The slip resistance, g^α, is composed of thermal (τ^*) and athermal (τ_{obs}) parts as follows [18]:

$$g^\alpha = \sqrt{(\tau^*)^2 + (\tau_\mathrm{obs})^2}, \tag{9}$$

where,

$$\tau^* = \tau_{cr} \left(1 - \left(\frac{k_b T}{H_0} \ln(\dot{\varepsilon}_0/\dot{\gamma}) \right)^{1/q} \right)^{1/p}, \quad \tau_\mathrm{obs} = A\mu \mathrm{b} \sqrt{\sum_{\beta=1}^{\mathrm{NS}} \rho^\beta}. \tag{10}$$

Here, T is the temperature, $\dot{\gamma}$ is the strain rate, H_0 is the activation enthalpy, k_b is the Boltzmann's constant, τ_{cr}, $\dot{\varepsilon}_0$ p, q and A are material constants, μ is the shear modulus, b is the Burger's vector, NS is the total number of slip systems, and ρ^β is the dislocation density on slip system β. Note that τ^* represents the temperature and strain rate dependent lattice resistance term based on dislocation-kink pair theory [29, 30, 6, 9, 18] while τ_obs is the athermal resistance to slip governed by dislocation-dislocation or dislocation-obstacle interactions. It is assumed that initial dislocation densities are identical for all 24 slip systems and the evolution of dislocation density for the α-th slip system is obtained by a standard phenomenological equation [16]. Detailed formulation of the model and material parameterizations for α-iron can be found in [20].

3 Results

A new capability to construct conformal hexahedral FE meshes using the phase field data is applied to three cases: (1) sphere grain embedded in a cubic grain, (2) two dimensional polycrystals and (3) three dimensional polycrystal structures. Plastic deformations of each case are conducted using CP-FEM model to investigate effects of conformal and conventional voxelated FE meshes on local mechanical behaviors or polycrystals.

3.1 Case I: Spherical grain within a cubic matrix

An idealized configuration of a spherical grain embedded inside a cubic grain is constructed using the phase field model as shown in Figure 5 (a). The total of 512,000 grids ($80\times80\times80$) and two order parameters, φ_1 and φ_2 were used to represent two grains. Outer cubic grain (Grain 1) is represented by φ_1=1 and φ_2=0, and interior sphere grain (Grain 2) is represented by φ_1=0 and φ_2=1. Interfaces between two grains, representing grain boundary regions, satisfy $0< \varphi_1 <1$ and $0< \varphi_2 <0$. Using the phase field data, two FE meshes, voxelated and conformal meshes, are generated as shown in Figure 5 (b). Here, the total of 512,000 and 540,248 eight-noded hexahedral finite elements are used to create voxelated and conformal meshes, respectively. The total of 30,047 and 44,171 finite elements are used to represent inner sphere grain (Grain 2) in voxelated and conformal meshes. It is shown that conformal mesh accurately represents smooth curvature of the sphere. On the other hand, Figure 6 (a) clearly shows limitation of the voxelated mesh in representing the smooth interface, even with relatively fine element sizes.

Two FE meshes shown in Figure 5 (b) are used to simulate uniaxial tension with CP-FEM model parameterized to α-iron. Initial crystal orientations of $\phi_1 = \Phi = \phi_2$=0 for Grain 1 and $\phi_1 = 90^\circ$, $\Phi = 135^\circ$ and $\phi_2 = 54.7^\circ$ for Grain 2 using Bunge Euler angles are assigned, respectively. Displacements along the x-direction are applied up to 10% engineering strain at a nominal strain rate of 10^{-4} s^{-1}. Figure 6 (a) shows simulated stress strain responses of the bicrystal using two FE meshes. It is shown that the mesh has negligible effect on the macroscopic response of bicrystals, less than 0.1 % deviation in engineering stress at 10 % deformation.

Figure 6 (b) shows von Mises stress distributions at 10 % deformation using voxelated and conformal FE meshes. It is shown that overall stress distributions through the thickness of Grain 1 is similar but higher stress localization is observed for voxelated mesh. To compare stress localizations quantitatively, Figure 7 illustrates von Mises stresses of the surface elements in Grain 2 at mid z-plane. Higher von Mises stress values along the surface of the Grain 2 are predicted using the voxelated FE mesh. The maximum von Mises stresses of the surface elements in Grain 2 at 10 % deformation are 121 MPa and 105 MPa for voxelated and conformal meshes, respectively. Thus, approximately 15 % deviation in the maximum von Mises stress is observed. Also note that the stress fields around the sphere grain is not continuous for the voxelated mesh. This result clearly shows that the voxelated mesh may induce spurious local stress localizations despite it is not clearly shown in global responses.

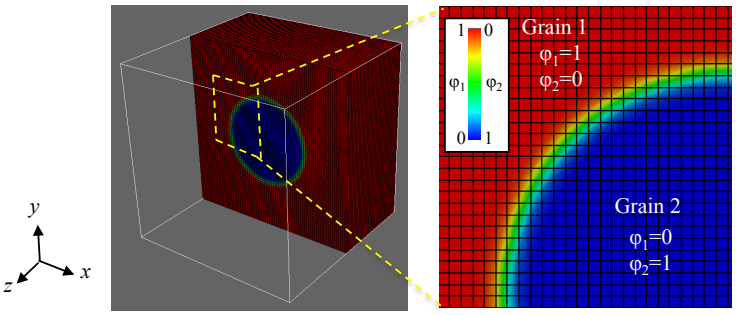

(a) Phase field data

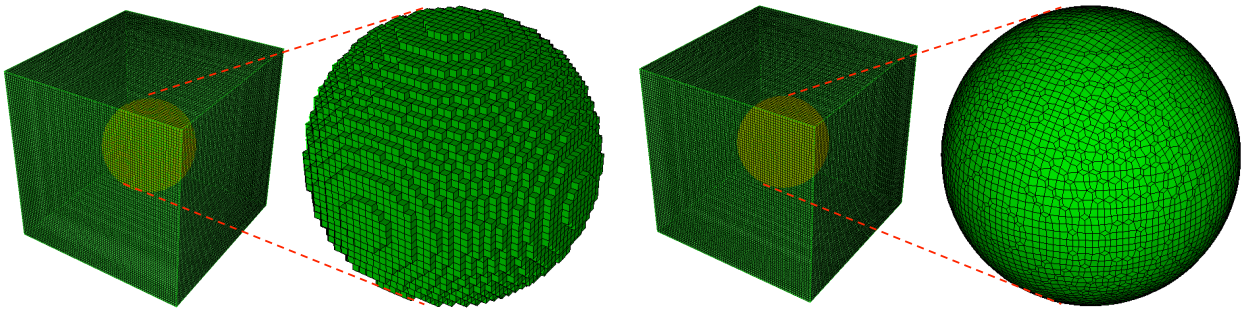

Voxelated FE mesh

Conformal FE mesh

(b) FE mesh

Figure 5. A sphere grain (Grain 2) embedded in a cubic grain (Grain 1). (a) Phase field representation of a cubic bicrystal specimen and (b) corresponding FE mesh using voxelated and conformal FE meshes.

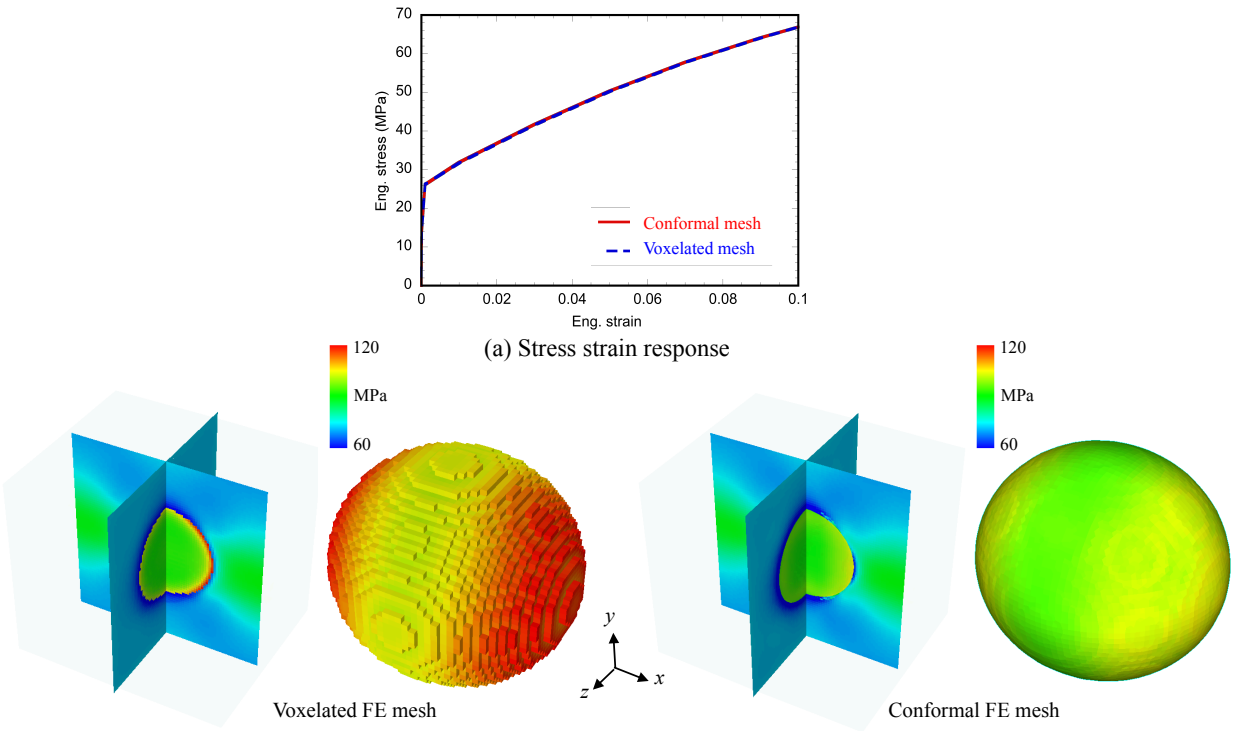

(a) Stress strain response

(b) VM stress at 10% deformation

Figure 6. Plots of (a) predicted stress-strain responses of bi-crystal specimens using conformal and voxelated meshes and (b) predicted von Mises stress after 10 % deformation along x direction.

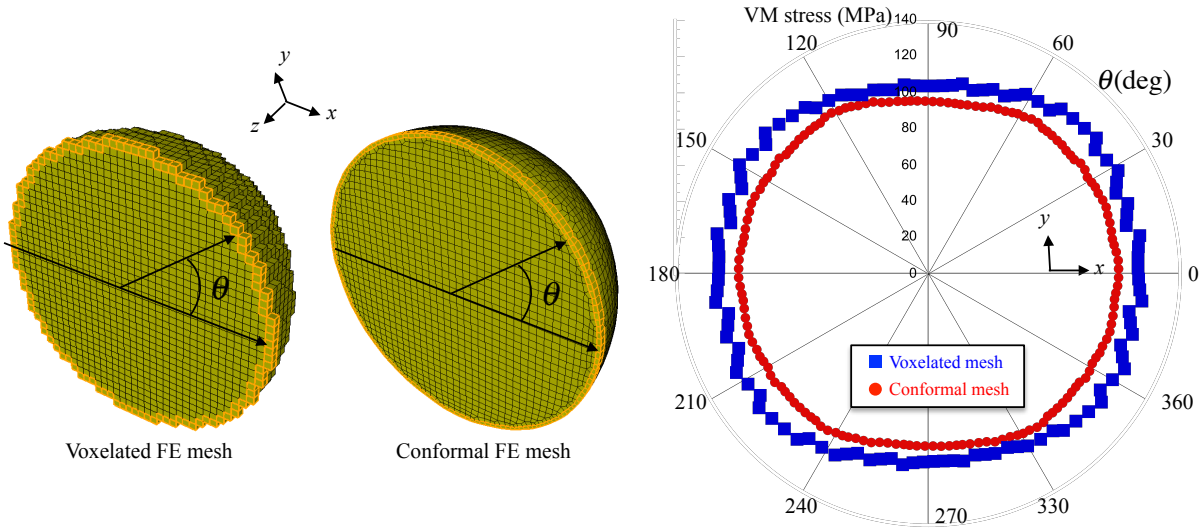

Figure 7. Predicted von Mises stress distribution in surface elements of the sphere grain (Grain 2) at the center of z-plane using voxelated and conformal finite element meshes at 10 % deformation.

3.2 Case II: Two-dimensional polycrystals

The second test case conducted in this work used series of two dimensional microstructure obtained from a phase field grain growth simulations. Different polycrystalline microstructures with varying grain sizes are obtained from different time steps of the grain growth simulation. The total of 131,072 ($256 \times 256 \times 2$) grids and 100 order parameters are used in the phase field simulation. Figure 8 shows snapshots of the polycrystalline microstructures from phase field grain growth simulations at four time steps having 16 - 127 grains. Grain boundaries are represented by $G = \sum_{i=1}^{n} \varphi_i^2 (1-\varphi_i)^2$ where, φ_i is the i^{th} order parameter and n is the total number of order parameters. Note that G is non-zero for grain boundary regions and zero for grain interior.

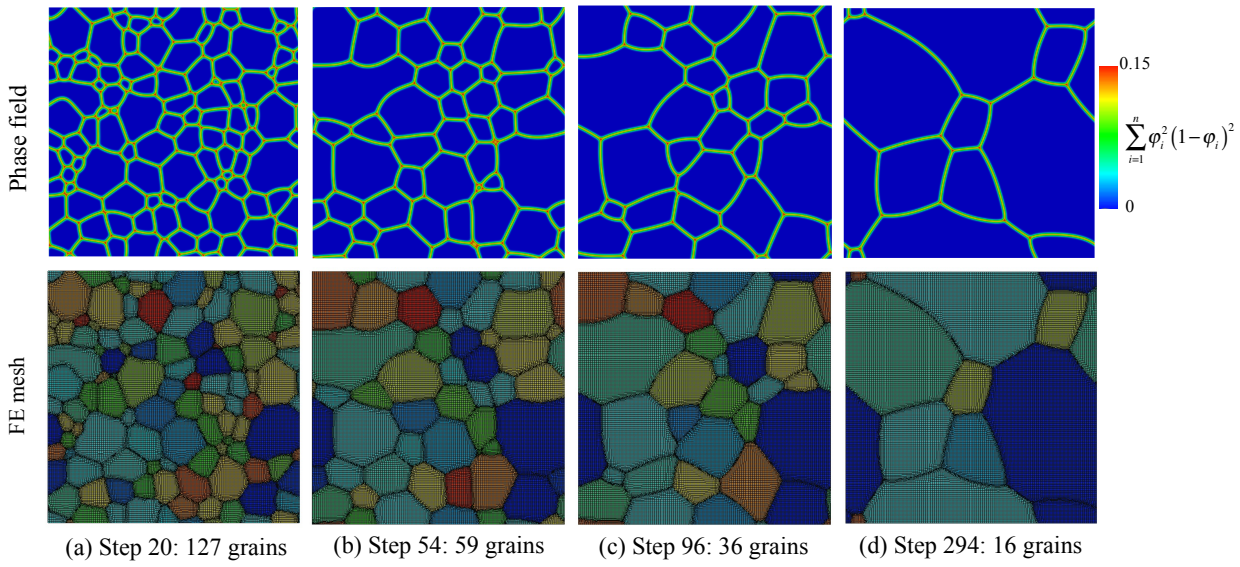

(a) Step 20: 127 grains (b) Step 54: 59 grains (c) Step 96: 36 grains (d) Step 294: 16 grains

Figure 8. Snapshots of microstructures from phase field grain growth simulations and corresponding FE meshes at various time steps having 16 - 127 grains.

Using four phase field results, corresponding conformal meshes having approximately 200,000 hexahedral FE are generated as shown in Figure 8. Two finite elements through the thickness (z-direction) are used to maintain good aspect ratios. Figures 9 (a) and (b) show one example of phase field data and corresponding finite element mesh at time step 20 having 127 grains. It is shown that approximately four grids are used to represent grain boundaries in the phase field model and the conformal mesh accurately reproduced curved grain boundaries and sharp triple junctions. Also note that triple junctions tend to form 120° between grain boundaries at all triple junctions which is not the case in most idealized representation of the polycrystalline microstructure, e.g. conventional Voronoi tessellations.

Similar to Case I, plastic deformations of four polycrystals are simulated using CP-FEM model.

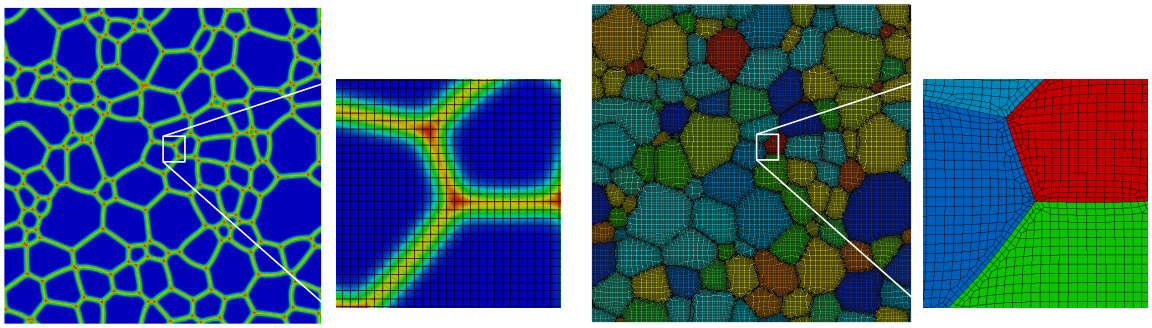

(a) Phase field data (b) Conformal FE mesh

Figure 9. Plots of (a) phase field grain growth model and (b) FE representation of the two dimensional polycrystals at time step 20 having 127 grains. Curved grain boundaries and sharp triple junctions are accurately reproduced by the conformal FE mesh.

Each grain is assigned with random initial crystal orientations and deformed up to 10% along x-direction. Figure 10 (a) shows predicted stress-strain responses of polycrystalline specimens having different number of grains and grain sizes. It is shown that flow stress is increased with the decreasing grain sizes or increasing grain numbers. Note however that the current plasticity model does not account for the effects of grain size on mechanical response, i.e. the Hall-Petch effect, which would require consideration of dislocation - grain boundary interactions. Observed distribution in macroscopic stress-strain response may attribute to local grain orientations and neighboring effects that alters local stress concentrations. This effect can be observed in Figure 10 (b), where von Mises stress distributions at 10 % deformation are compared for different microstructures. It is shown that the more localized stress is observed near the grain boundaries and triple junctions and their effects are more significant for microstructures having more grains.

The procedure outlined above is a promising method to directly connect thermodynamically driven grain growth model to mechanics simulation. In particular, local phenomena near the grain boundary can be better investigated by physically-based representation of the polycrystalline domain and finite element meshes that conform to boundaries [8].

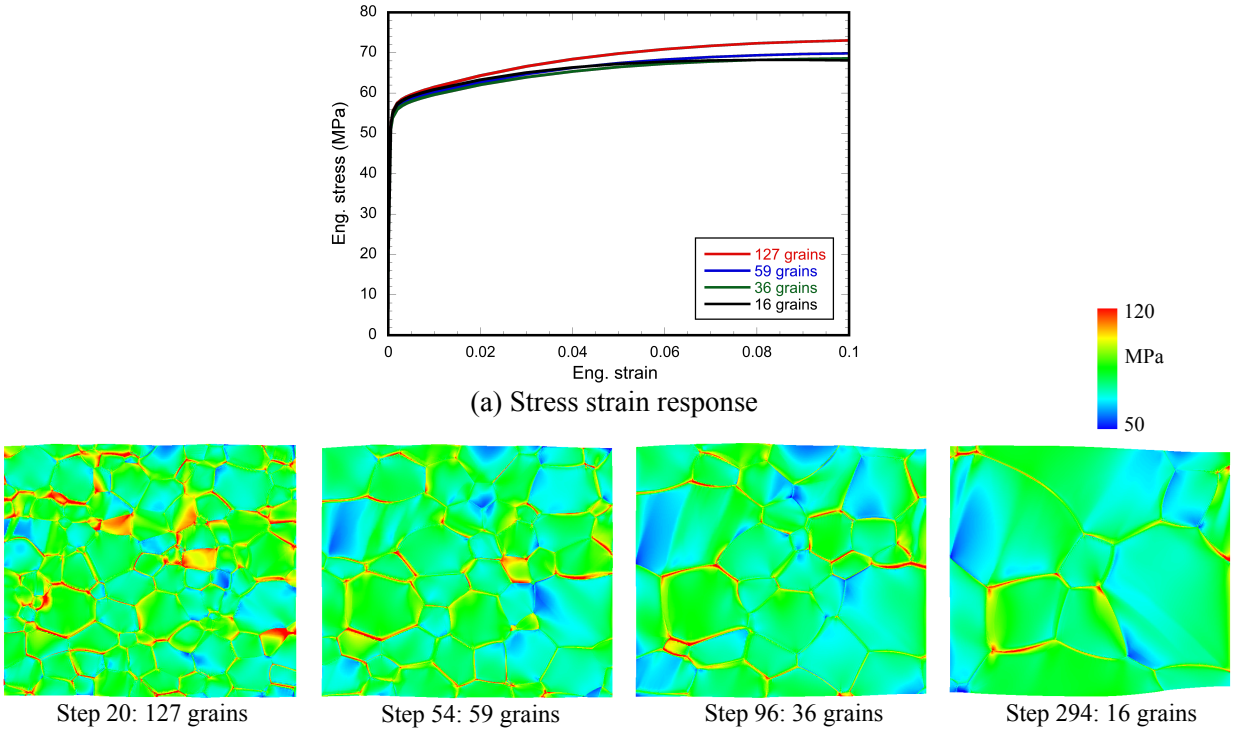

(a) Stress strain response

(b) VM stress at 10% deformation

Figure 10. Plots of (a) predicted stress strain responses of polycrystals and (b) von Mises stresses at 10% deformation having 127 grains, 59 grains, 36 grains and 16 grains. Stress localizations are observed near the grain boundaries and triple junctions.

3.3 Case III: Three dimensional polycrystals

A three dimensional polycrystalline microstructure is constructed using the phase field grain growth simulation as shown in Figure 11 (a). The totals of 884,736 grids (96×96×96) and 20 order parameters are used to represent 52 grains. Using the phase field data, voxelated and conformal meshes are constructed with 884,736 and 1,277,808 hexahedral elements, respectively. Figure 11 (b) shows FE meshes of a polycrystalline and one grain at the center of the domain (Grain 9) using two meshing techniques. Similar to simplified cases, Case I and II in the previous sections, smooth surfaces of individual grain are accurately captured by the conformal mesh.

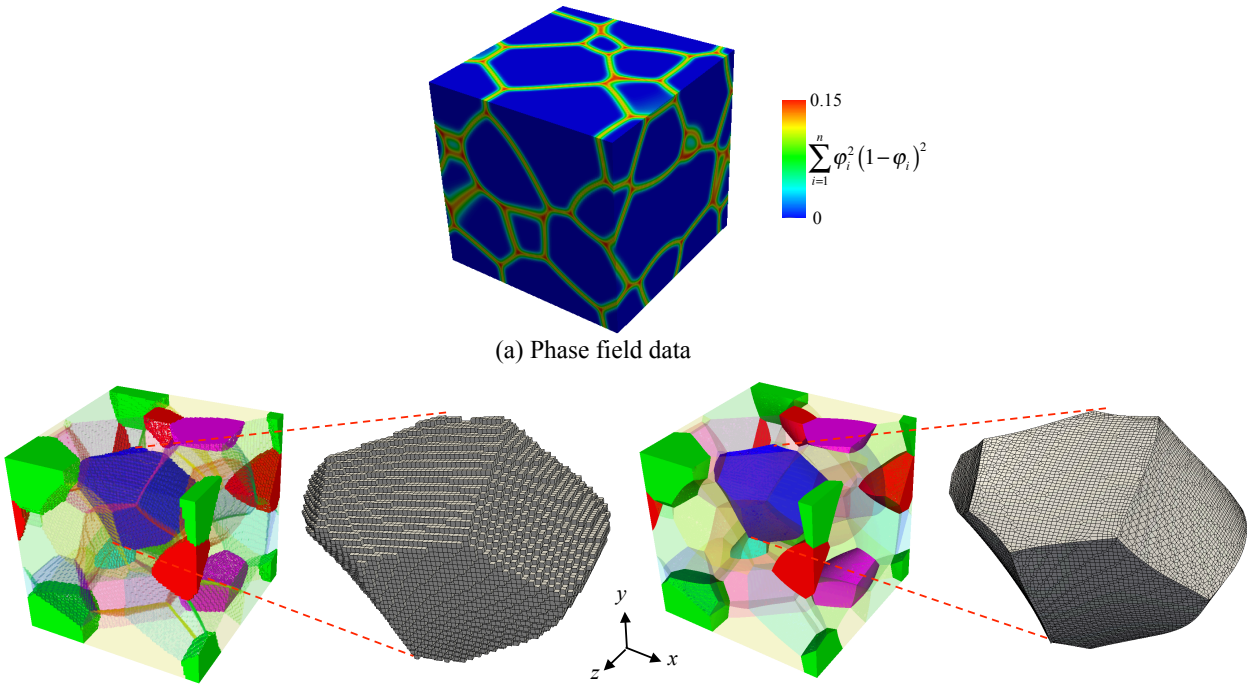

(a) Phase field data

(b) FE mesh

Figure 11. Three dimensional polycrystalline microstructure constructed from (a) phase field data and (b) FE representation of the polycrystal using voxelated and conformal meshing techniques.

Uniaxial tensions of the three dimensional polycrystalline specimen are simulated using voxelated and conformal FE meshes. Displacements along the x-direction are applied up to 10 % engineering strain at a nominal strain rate of 10^{-4} s^{-1}. Figures 12 (a) and (b) show predicted stress strain response and von Mises stress distributions using two FE meshes, respectively. Similar to Case I, CP-FEM simulations using conformal and voxelated meshes show relatively small difference in macroscopic response. On the other hand, Figure 12 (b) illustrates that the confor-

mal mesh can resolve more detailed stress distributions, especially near the grain boundaries and triple junctions. This may attributed to interface conformal mesh as well as finer elements near the boundaries, generated from the Sculpt operation. More importantly, as clearly shown in Grain 11, the conformal mesh eliminates spurious stress localizations observed at the grain surface in voxelated mesh.

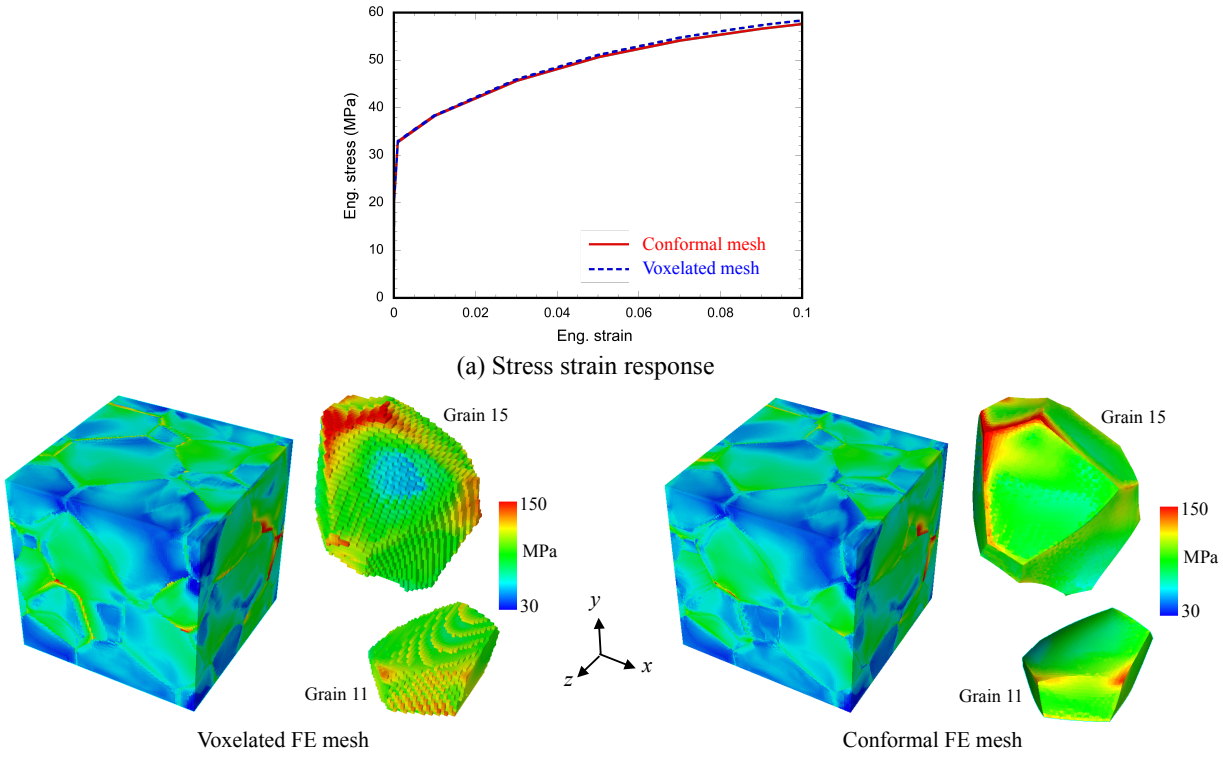

(a) Stress strain response

(b) VM stress at 10% deformation

Figure 12. Predicted stress strain responses and von Mises stress distributions von Mises stress distributions at 10 % deformation using (a) voxelated and (b) conformal meshes.

In order to quantitatively compare inter and intra-granular local stress fields predicted from two meshing techniques, von Mises stresses profiles along the x-direction at mid z-plane are obtained as shown in Figure 13. Note that A and B correspond to a grain boundary and triple junction within a polycrystalline microstructure. It is shown that von Mises stress predictions using two meshes show similar distributions inside the grain while relatively large deviations were observed near the grain boundary (point A) and triple junction (point B). In particular, voxelated mesh showed large stress localization near the triple junction; von Mises stress values are 78 MPa and 128 MPa at point B for the conformal and voxelated meshes, respectively. This result again exhibits that voxelated mesh may induce incorrect stress localizations and may not be suitable for modeling local phenomena.

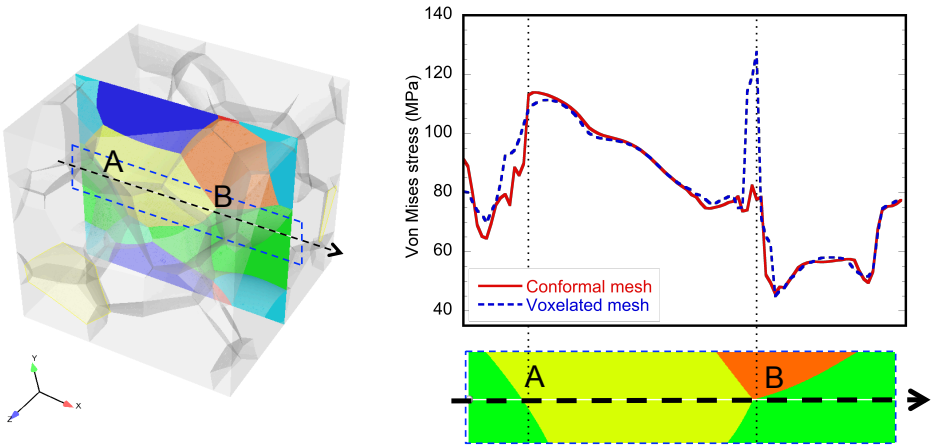

Figure 13. Predicted von Mises stress profiles along the x-direction at mid z-plane of the specimen using the conformal mesh and voxelated mesh. Von Mises stress profiles along the dashed lines are plotted at 10 % deformation.

In addition to local mechanical responses, effects of mesh on texture evolution is investigated by plotting crystal orientations before and after in rolling direction (RD), transverse direction (TD) and normal direction (ND) within the unit stereographic triangle. Figure 14 shows plots of initial (black data points) and deformed texture (color contours). Here, an occurrence of crystal orientation data within a unit area of the stereographic triangle is normalized by the random occurrence. The spread in the initial crystal orientations within a grain are observed in the deformed texture. Similar to macroscopic stress-strain response, overall predicted texture using voxelated and conformal FE meshes show good agreement. However, crystal orientations tend to spread more for a conformal mesh. This may attribute to interface conformal elements near the grain boundaries that accommodate larger crystal rotations.

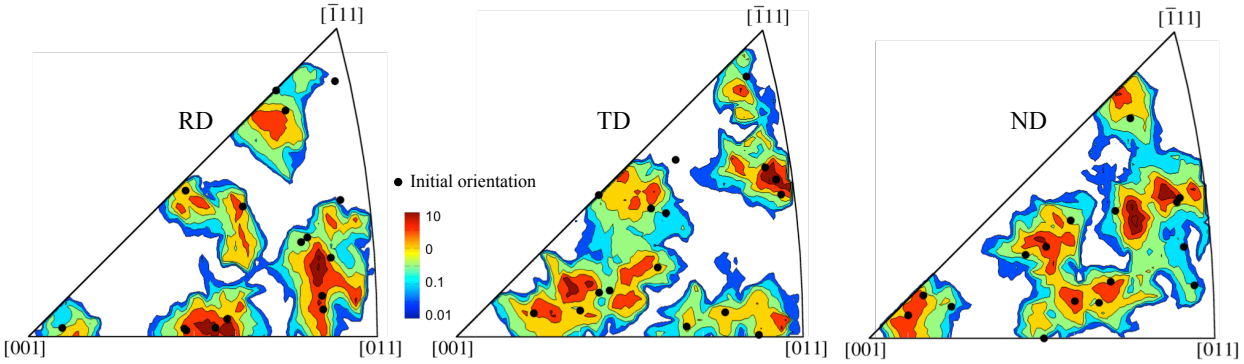

(a) Voxelated FE mesh

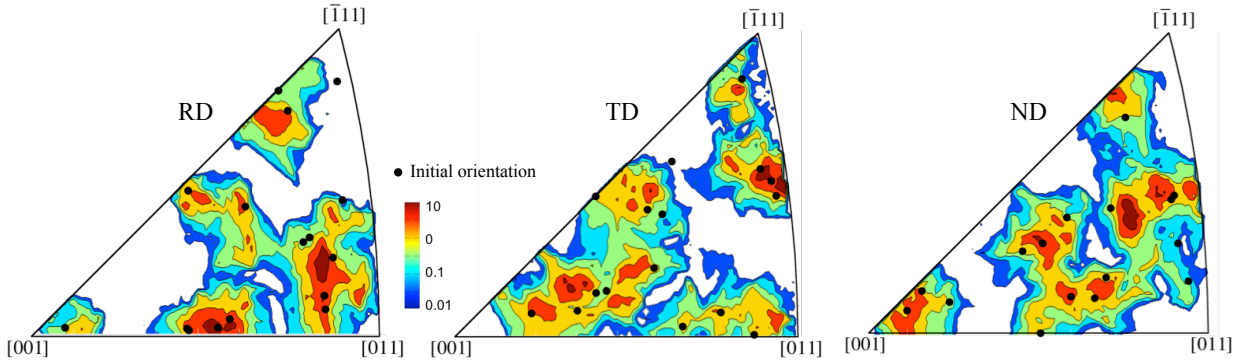

(b) Conformal FE mesh

Figure 14. Predicted texture density plots from CP-FEM predictions using (a) voxelated and (b) conformal FE meshes. Color scale represents the multiple times random occurrence at 10% deformation.

4 Discussion

4.1 Mesh sensitivity

In FE-based simulations, mesh refinement and sensitivity can play an important role in predicting material's response. In order to investigate mesh sensitivities of both voxelated and conformal meshes, three dimensional polycrystalline microstructure is created using the phase field grain growth simulation. A total of 884,736 grids (96×96×96) are used to construct a polycrystal with 47 grains. Phase field data is then used to create FE meshes with varying element sizes. Figures 15 (a) and (b) show hierarchical refinement using both voxelated and conformal meshing approaches. Voxelated meshes denoted as Mesh (v1) - (v5) have total numbers of 4,096 to 884,736 elements and conformal meshes (c1- c5) have 17,730 to 1,281,856 elements as listed in Table 1.

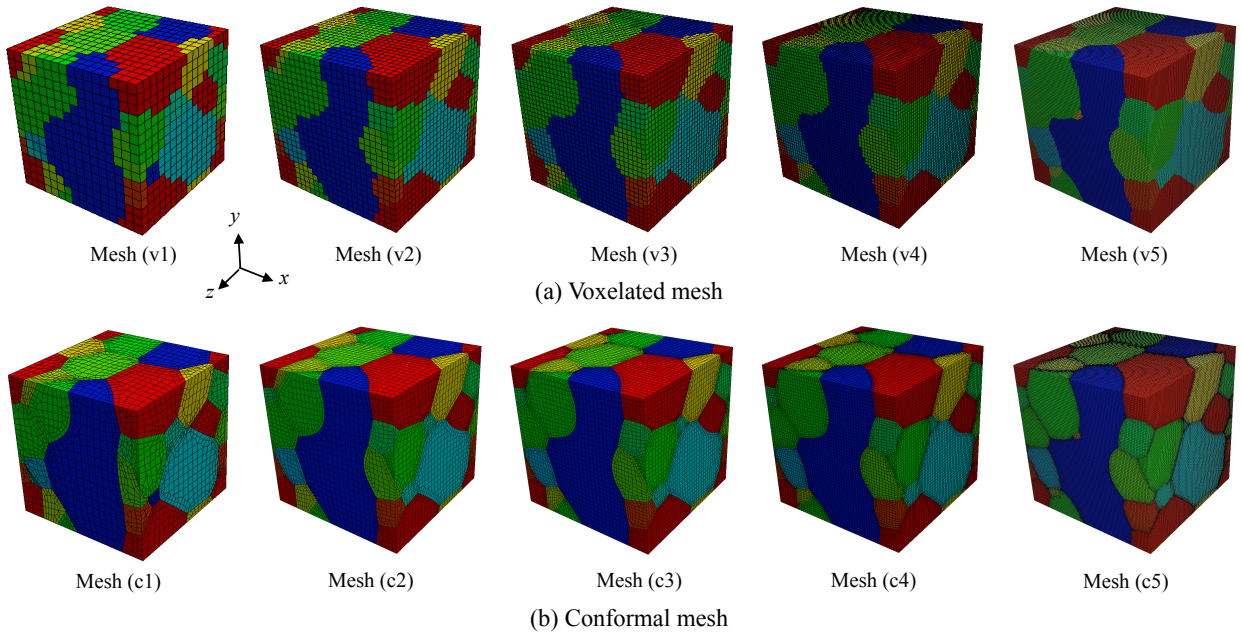

Figure 15. Initial finite element meshes with hierarchical refinements using (a) voxelated and (b) conformal meshing techniques.

Similar to CP-FE simulations conducted in the previous chapter, each mesh is used to simulate uniaxial tension up to 10 % deformation. Figure 16 (a) shows stress strain responses of polycrystals having voxelated and conformal FE meshes. It is shown that the flow stress did not converge with meshes up to 10^6 elements. It should be noted that CP-FEM simulations of single crystals having the same number of elements as Figure 15 showed negligible mesh dependence on stress-strain behavior. Thus, in polycrystalline FE simulations, numbers of elements that represent each grain is important as well as the total number of elements representing the whole domain. Figure 16 (b)

Table 1. Predicted flow stress and local von Mises stress values using different FE meshes.

Mesh ID	Total number of elements	Elements per grain	Flow stress (MPa) 0.2%	5%	10%	VM stress at 20% (MPa) min.	max.
v1	4,096	87	76.7	104.2	110.6	76.3	264.2
v2	13,824	294	76.1	101.3	106.5	67.7	249.4
v3	32,768	697	75.8	99.6	103.9	65.2	258.4
v4	110,592	2,353	75.5	97.7	100.9	57.5	266.3
v5	884,736	18,824	75.3	95.6	97.4	52.2	287.3
c1	17,730	377	75.1	100.3	106.0	66.4	247.7
c2	42,922	913	74.7	97.7	102.2	62.2	257.6
c3	81,838	1,741	74.6	96.6	100.2	59.8	261.1
c4	215,714	4,590	74.6	95.3	97.9	55.3	271.9
c5	1,281,856	27,274	74.7	94.1	95.5	47.7	328.1

shows effects of mesh refinement on the yield stress (0.2 % strain offset) and the flow stress at 10 % deformation. At both strain levels, conformal mesh showed faster mesh convergence compared to voxelated mesh. In particular, conformal mesh showed better convergence rate at low strain level.

Figures 17 (a) and (b) show predicted von Mises stress distributions at mid z-plane after 10 % deformation using two meshing techniques. As expected, voxelated meshes, even with very fine FE size, could not avoid mesh-dependent pixelated stress fields near the curved boundaries. In addition, using the similar numbers of elements, e.g. meshes (v2) - (c1), conformal mesh resolved finer stress distributions compared to voxelated mesh.

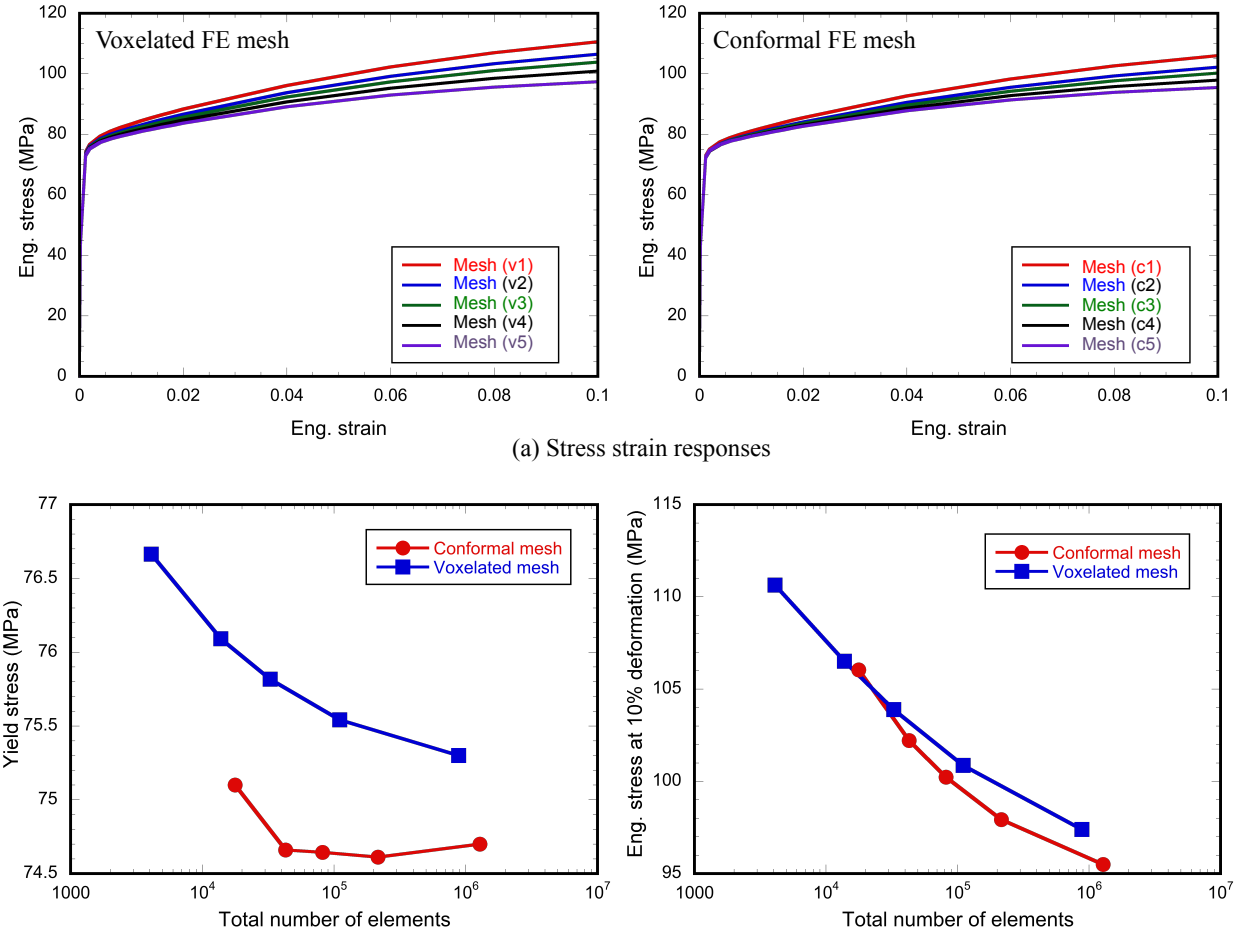

(a) Stress strain responses

(b) Flow stresses at 0.2% and 10% deformation

Figure 16. Plots of (a) predicted stress strain responses with mesh refinements and (b) flow stresses at 0.2 % and 10 % deformations.

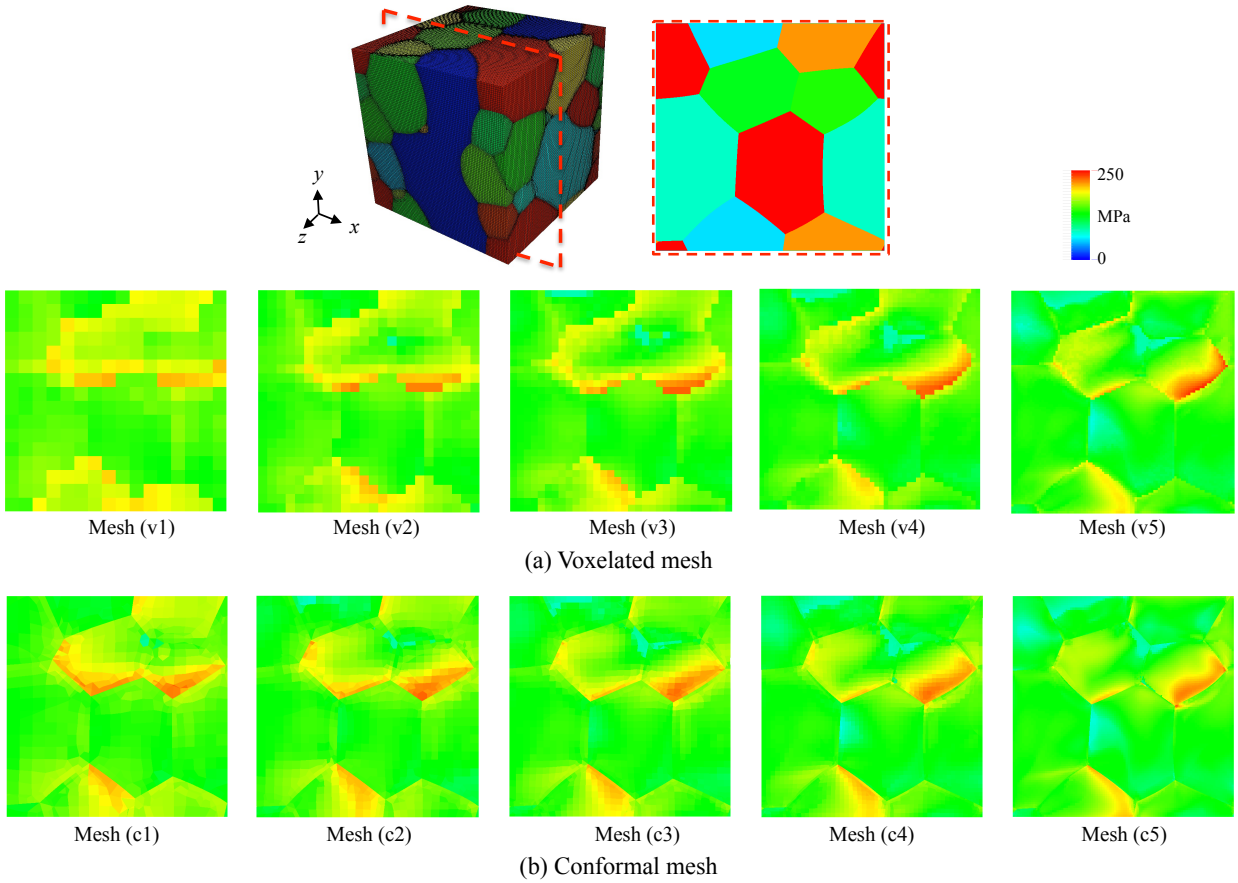

Figure 17. Predicted von Mises stress distributions at mid z-plane after 10 % deformation using (a) voxelated meshes and (b) conformal meshes.

4.2 Anticipated impact

In addition to using phase field data to create conformal finite element meshes, Sculpt operation in Cubit can be extended to generate interface reconstructions from various sources, e.g. electron backscatter diffraction (EBSD), Monte Carlo models or other non-conformal finite element meshes. Figure 18 shows extended applications of the conforming meshing technique. Figure 18 (a) shows conformal mesh generated from the voxelated mesh (Exodus format) and Figure 18 (b) represents FE mesh generated from Monte Carlo potts grain growth simulations having two phase structure. This meshing technique can be applied to any other three dimensional computational models or experimental data to construct interface-conformal microstructures.

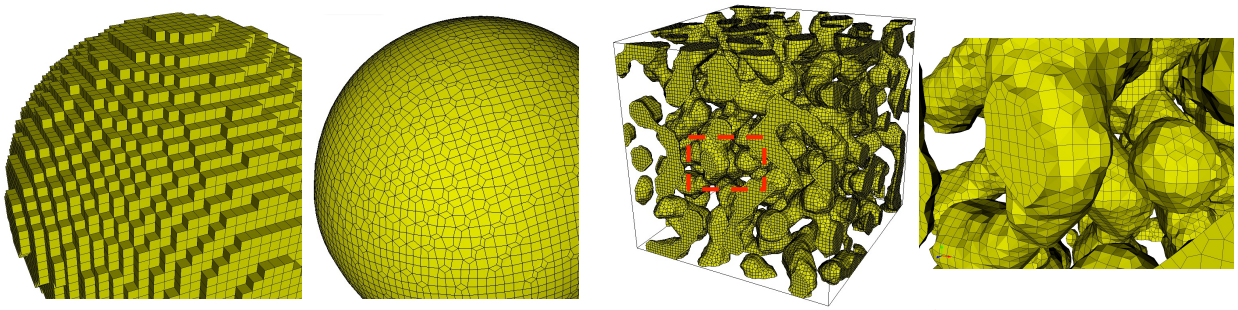

(a) (b)

Figure 18. Extended applications of the conformal meshing technique. Conformal meshes are generated from (a) voxelated finite element mesh and (b) Monte Carlo potts grain growth simulation results.

The current work in Case III showed mechanical simulation of three dimensional polycrystals having 47 grains and 1.3 million elements that may not be sufficient to represent engineering scale polycrystals. More robust performance and mesh quality will enable scaling up to realistic numbers of grains and component-scale modeling. Figure 19 shows one example of large-scale three dimensional polycrystalline phase field data and corresponding conformal mesh. A total of 7,077,888 hexahedral finite element elements are used to represent 329 grains. Polycrystalline mesh of this size have enough number of grains to represent true polycrystalline behaviors. In order further extend this capability, large-scale parallelization in high-performance computing systems and optimization studies to efficiently construct and simulate polycrystalline microstructure are anticipated. Large-scale polycrystalline simulations using realistic microstructures will allow us to investigate microstructural variability, performance and reliability of engineering applications in a manner that requires less time and expense than conventional approaches.

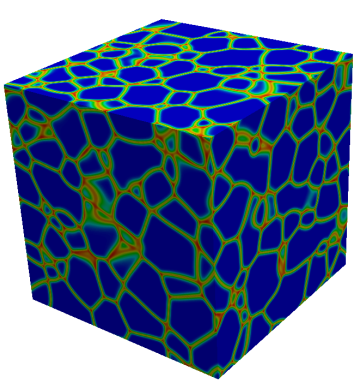

(a) Phase field data

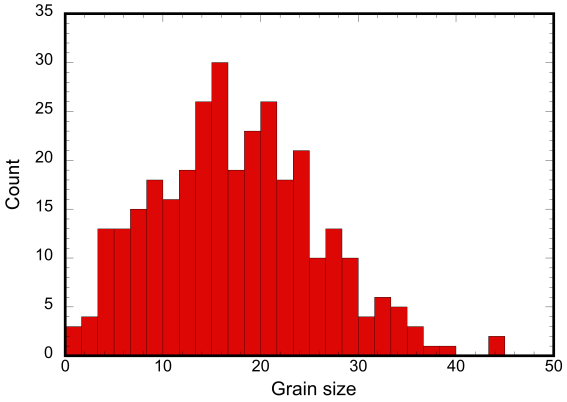

(b) Grain size distribution

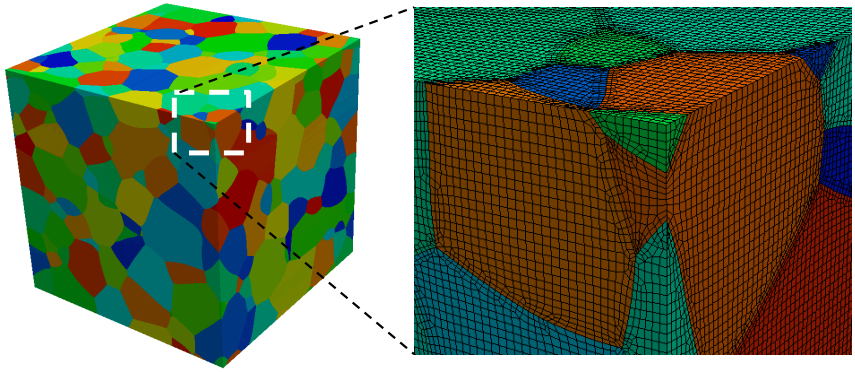

(c) Conformal FE mesh

Figure 19. Large-scale three dimensional polycrystalline phase field data and conformal mesh. A total of 7,077,888 hexahedral finite elements were used to represent 522 grains.

5 Conclusion

Concurrent trends in a wide variety of technologies are moving towards component miniaturization and increased realism in predictive simulations. This necessitates microstructure-aware engineering analysis capabilities for a variety of applications. In order to better incorporate microstructures in continuum scale models, the new meshing technique described in this report uses phase field grain growth results to create physically realistic polycrystalline meshes with hexahedral finite elements. In addition, the new mesh technique constructs smooth interfaces between adjacent grains to capture realistic grain boundary morphology.

The current work showed that the global response of the polycrystal, i.e. stress strain response and texture, is not significantly affected by the accurate modeling of interfaces. However, localized stress values are largely affected by the mesh near the interfaces. It is shown that voxelated mesh near interfaces may cause large stress localizations or unrealistic stress distributions. This effect became more pronounced with the increased complexity of the microstructure. Thus, FE models that consider localized events such as damage, crack and fracture, may require using interface conformal mesh.

This effort will deliver a practical computational capability based on materials science needs, and will enable more realistic engineering-scale simulations of polycrystalline metals for a variety of applications. Further extension of this work will anticipate fundamental materials design and synthesis of application-optimized microstructures.

References

[1] F. Abdeljawad and S. M. Foiles. Stabilization of nanocrystalline alloys via grain boundary segregation: A diffuse interface model. 2015. . Submitted to Acta Mater.

[2] F. Abdeljawad, B. Voelker, R. Davis, R. M. McMeeking, and M. Haataja. Connecting microstructural coarsening processes to electrochemical performance in solid oxide fuel cells: An integrated modeling approach. *J. Power Sources*, 250:319–331, 2014.

[3] S. M. Allen and J. W. Cahn. A microscopic theory for antiphase boundary motion and its application to antiphase domain coarsening. *Acta Metall.*, 27(6):1085–1095, 1979.

[4] L. Anand and S. R. Kalidindi. The process of shear-band formation in plane- strain compression of fcc metals - effects of crystallographic texture. *Mechanics of Materials*, 17:223–243, 1994.

[5] Y. Aoyagi and K. Shizawa. Multiscale crystal plasticity modeling based on geometrically necessary crystal defects and simulation on fine-graining for polycrystal. *International Journal of Plasticity*, 23:1022–1040, 2007.

[6] A. Argon. *Strengthening mechanisms in crystal plasticity*. Oxford University Press, 2008.

[7] F. Barbe, L. Decker, D. Jeulin, and G. Cailletaud. Intergranular and intragranular behavior of polycrystalline aggregates. *p*art 1: $f.e.$ model. *International Journal of Plasticity*, 17:513–536, 2001.

[8] C. C. Battaile, W. A. Counts, G. W. Wellman, T. E. Buchheit, and E. A. Holm. Simulating grain growth in a deformed polycrystal by coupled finite-element and microstructure evolution modeling. *Metallurgical and Materials Transactions A*, 38A:2513–2522, 2007.

[9] M. Z. Butt. Kinetics of flow stress in crystals with high intrinsic lattice friction. *Philos. Mag.*, 87:3595–3614, 2007.

[10] P. R. Dawson, S. R. MacEwen, and P. D. Wu. Advances in sheet metal forming analyses: dealing with mechanical anisotropy from crystallographic texture. *International Materials Reviews*, 48:86–122, 2003.

[11] F. Delaire, J. L. Raphanel, and C. Rey. Plastic heterogeneities of a copper multicrystal deformed in uniaxial tension: Experimental study and finite element simulations. *Acta Mater.*, 48:1075–1087, 2000.

[12] R. Dingreville, C. C. Battaile, L. N. Brewer, E. A. Holm, and B. L. Boyce. The effect of microstructural representation on simulations of microplastic ratcheting. *Int. J. Plasticity*, 21:617–633, 2010.

[13] R. Hill and J. R. Rice. Constitutive analysis of elastic plastic crystals at arbitrary strain. *J. Mech. Phys. Solids*, 20:401–413, 1972.

[14] J. W. Hutchinson. Bounds and self-consistent estimates for creep of polycrystalline materials. *Proc. R. Soc. Lond. A*, 348:101–127, 1976.

[15] S. R. Kalidindi, C. A. Bronkhorst, and L. Anand. Crystallographic texture evolution in bulk deformation processing of fcc metals. *J. Mech. Phys. Solids*, 40:537, 1992.

[16] U. F. Kocks. Laws for work-hardening and low-temperature creep. *J. Eng. Mater. Tech., ASME*, 98:76–85, 1976.

[17] E. H. Lee. Elastic-plastic deformation at finite strains. *Appl. Mech.*, 36:1–6, 1969.

[18] H. Lim, C. C. Battaile, J. D. Carroll, B. L. Boyce, and C. R. Weinberger. A physically based temperature and strain rate dependent crystal plasticity model for bcc metals. *J. Mech. Phys. Sol.*, 74:80–96, 2015.

[19] H. Lim, J. D. Carroll, C. C. Battaile, T. E. Buchheit, B. L. Boyce, and C. R. Weinberger. Grain-scale experimental validation of crystal plasticity finite element simulations of tantalum oligocrystals. *Int. J. Plasticity*, 60:1–18, 2014.

[20] H. Lim, L. M. Hale, Z. A. Zimmerman, C. C. Battaile, and C. R. Weinberger. A multi-scale model of dislocation plasticity in α-Fe: Iincorporating temperature, strain rate and non-schmid effects. *Int. J. Plasticity*, In press, 2015.

[21] H. Lim, C. R. Weinberger, C. C. Battaile, and T. E. Buchheit. Application of generalized non-Schmid yield law to low temperature plasticity in bcc transition metals. *Model. Simul. Mater. Sci. Eng.*, 21:045015, 2013.

[22] F. Meier, C. Schwarz, and E. Werner. Crystal-plasticity based thermo-mechanical modeling of al-components in integrated circuits. *Computational Materials Science*, 94:122–131, 2014.

[23] S. J. Owen. Parallel smoothing for grid-based methods. *Proceedings 21st International Meshing Roundtable*, page Research Notes, 2013.

[24] S. J. Owen, M. L. Staten, and M. C. Sorensen. Parallel hex meshing from volume fractions. *Proceedings 20th International Meshing Roundtable*, pages 161–178, 2011.

[25] D. Peirce, R. J. Asaro, and A. Needleman. An analysis of nonuniform and localized deformation in ductile single crystals. *Acta Metall.*, 30:1087–1119, 1982.

[26] D. Pyle, J. Lu, D. J. Littlewood, and A. M. Maniatty. Effects of $3d$ grain structure representation in polycrystal simulations. *Computational Mechanics*, 52:135–150, 2012.

[27] D. Raabe, Z. Z. M. Sachtleber, F. Roters, and S. Zaefferer. Micromechanical and macromechanical effects in grain scale polycrystal plasticity experimentation and simulation. *Acta Mater.*, 49:3433–3441, 2001.

[28] J. R. Rice. Inelastic constitutive relations for solids, an internal-variable theory and its application to metal plasticity. *J. Mech. Phys. Solids*, 19:443–455, 1971.

[29] A. Seeger. The temperature and strain-rate dependence of the flow stress of body-centered cubic metals: A theory based on kink–kink interactions. *Z. Metallikd*, 72:369–380, 1981.

[30] A. Seeger. Why anomalous slip in body-centred cubic metals? *Mater. Sci. Eng. A*, 319-321:254–260, 2001.

[31] M. Zhang, J. Zhang, and D. L. McDowell. Microstructure-based crystal plasticity modeling of cyclic deformation of *t*i6*a*l4*v*. *International Journal of Plasticity*, 23:1328–1348, 2007.

[32] Z. Zhao, M. Ramesh, D. Raabe, A. Cuitiño, and R. Radovitzky. Experimental investigation of plastic grain interaction. *Int. J. Plasticity*, 24:2278–2297, 2008.

DISTRIBUTION:

1	MS 0889	Corbett Battaile, 01814
1	MS 0897	Byron Hanks, 01543
1	MS 1114	Steven Owen, 01543
1	MS 1411	Hojun Lim, 01814
1	MS 1411	Fadi Abdeljawad, 01814
1	MS 9042	James Foulk III, 08256
1	MS 0899	Technical Library, 09536

Sandia National Laboratories